Journal of Mathematical Chemistry Vol. 28, No. 4, 2000

Dynamical analysis of an elementary $X + Y \rightarrow P$ reaction in a continuously stirred tank reactor

H.S. Sidhu, M.I. Nelson, G.N. Mercer and R.O. Weber

School of Mathematics and Statistics, University College, University of New South Wales, Australian Defence Force Academy, Canberra 2600, Australia

Received 3 October 2000

This paper investigates the bifurcation behaviour of a model oxidation reaction in a continuously stirred tank reactor (CSTR). We assume that two gaseous chemical species are pumped separately into the CSTR, at constant total pressure, reacting to produce an inert product. The reaction is assumed to be a single step reaction that is described by Arrhenius kinetics. It is capable of producing oscillatory behaviour as well as steady state multiplicity in certain parameter regions. Bifurcation diagrams in various control parameter spaces are presented. We show that the system always possesses a globally attracting invariant region. The equivalence of a CSTR having n feed streams and the one pipe version, by appropriate rescaling, is also discussed.

KEY WORDS: exothermic reaction, bifurcation, flammability limits, flow reactor

1. Introduction

The continuously stirred tank reactor (CSTR) is a well documented experimental and theoretical tool for studying chemical reactions [1–3]. The principal virtues of the CSTR are that elementary and complex reactions can be studied in a simple arrangement, which is repeatable in different laboratories and allows the utilisation of several convenient control variables. The control variables most frequently exploited are the flow rate of reactants into the CSTR, the initial temperature of the reactants prior to entering the CSTR, the ambient temperature of the oven in which the CSTR is located, and the relative proportions or concentrations of the reactants fed into the CSTR.

The classical first-order, non-isothermal scheme (sometimes referred to as FONI) in the well stirred, flow reactor scenario has been extensively studied by numerous authors over the years (see, for example, Zeldovich [4], van Heerden [5], Bilous and Amundson [6], Aris and Amundson [7–9], Hlavacek et al. [10], Uppal et al. [11,12], Balakotaia and Luss [13–18], Farr and Aris [19], Planeaux and Jensen [20] and more recently by Ball and Gray [21]). This simple exothermic scheme (a single reaction which converts a reactant to an inert product) has been shown to possess a variety of dynamical behaviour, from stationary-state curve that has isolas, mushrooms and hysteresis

0259-9791/00/1200-0353$18.00/0

loops, to Hopf bifurcations (both the supercritical and subcritical type) and homoclinic orbits.

In this paper we extend the above scheme to incorporate *two* incoming reactants (a fuel species and oxygen) rather than just the one reactant assumed in the FONI scheme. The two reactants are pumped separately into the CSTR and react to produce an inert product. The primary aim of this paper is to investigate the dynamical behaviour of this prototypical oxidation scheme. Furthermore, we are also interested in using this scheme to undertake a preliminary investigation of flammability limits in the CSTR.

For gaseous reactants (as assumed in this investigation), the total pressure is an important quantity and is kept fixed in combustion experiments pertaining to flammability limits of gaseous fuels (see Drysdale [22], Baulch et al. [23] and Johnson et al. [24]). The partial pressures of the incoming fuel, oxygen and an inert gas (normally nitrogen) may then be varied to determine the critical lower (fuel-lean) limit and the upper (fuel-rich) flammability limits. This leads naturally to considering the relative proportions of gaseous reactants as they are fed into the CSTR; which in turn prompts us to expect flammability limits.

The exothermic reaction considered in this paper is modelled as a single-step, irreversible reaction where the rate is temperature dependent according to the Arrhenius formula. The assumption of a global reaction rate is convenient for the mathematical analysis of the CSTR model. Reduced kinetic schemes have been used with success in reaction modelling (for example, the 33 steps involving 8 species for H_2–O_2 presented by Baulch et al. [23] and the reduced 10 step system by Johnson et al. [24], or the numerous examples given by Williams [25] in his monograph).

We begin the study in section 2 by introducing the mathematical model. Following non-dimensionalisation, the global dynamics of the governing equations is studied and a region of ultimate confinement is established. The steady states are determined and their stability classified in section 3. This is an essential first step in understanding the dynamics of the model. Multiplicity in the steady states and oscillatory solutions occur for certain parameter values, the latter arising through Hopf bifurcations. Bifurcation diagrams in the control parameter space showing regions of multiple steady state solutions as well as oscillatory solutions are presented in section 4.

A brief discussion of how the dynamical investigation presented previously can be interpreted in terms of flammability limits is presented in section 5. Here we have assumed that no inert species such as nitrogen is present in the scheme (only fuel and oxygen). The discussion of our detailed investigation of the flammability limits of oxygen–fuel–inert mixtures in a CSTR is presented elsewhere [26]. Appendix A provides details regarding the equivalence of the CSTR with two inflow pipes (i.e., having two feed streams into the reactor), like the one considered in this paper, to the one pipe version when the inflow and outflow rates as well as the input concentrations of the chemicals are rescaled. The results presented here can easily be extended to include a CSTR with any number of inflow pipes. Such a situation can arise when investigating the flammability of mixtures of fuels all of which can react with each other.

2. Governing equations

We consider the simple reaction

$$\mathrm{X} + \mathrm{Y} \rightarrow \mathrm{P}, \tag{1}$$

taking place in a CSTR with volume V. Here both the reactants X and Y are fed into the reactor separately (through two inflow pipes) with volume flow rate k_{f}' via pre-heating coils so that they are both at the oven temperature T_{a} before entry. The end products of this reaction are denoted by P. Assuming that the exothermic reaction is temperature dependent and behaves in accordance with Arrhenius kinetics, the mathematical description of the progress of the reaction (1) is described by the rate equations

$$\begin{aligned} \frac{\mathrm{d}[\mathrm{X}]}{\mathrm{d}t'} &= \frac{k_{\mathrm{f}}'}{V}[\mathrm{X}]_0 - [\mathrm{X}][\mathrm{Y}]A\mathrm{e}^{-E/RT} - \frac{2k_{\mathrm{f}}'}{V}[\mathrm{X}], \\ \frac{d[\mathrm{Y}]}{\mathrm{d}t'} &= \frac{k_{\mathrm{f}}'}{V}[\mathrm{Y}]_0 - [\mathrm{X}][\mathrm{Y}]A\mathrm{e}^{-E/RT} - \frac{2k_{\mathrm{f}}'}{V}[\mathrm{Y}], \end{aligned} \tag{2}$$

where the notation [X] and [Y] denotes the reactant concentrations of chemical X and Y, respectively, T is the temperature of the reaction and t' denotes time. The concentrations of chemicals X and Y at the inflow are represented by $[\mathrm{X}]_0$ and $[\mathrm{Y}]_0$, respectively. For simplicity the reaction kinetics are defined in terms of a global Arrhenius rate that is first order with respect to the reactants. In practice the activation energy (E), the pre-exponential factor (A), and the heat of reaction ($-\Delta H$) in a global reaction rate depend upon the composition of the reactant mixture (for example, see [27]). For simplicity the above-mentioned parameters in this investigation are assumed to be independent of the composition.

As in the case of many experimental situations (see, for example, Baulch et al. [23] and Johnson et al. [24,28]), we shall assume that the well-stirred flow reactor (with volume V and surface area S) is placed in an oven maintained at a temperature T_{a}. The contents in the reactor are assumed to have density σ and molar heat capacity c_v at constant volume. The energy balance equation for our model is

$$\sigma V c_v \frac{\mathrm{d}T}{\mathrm{d}t'} = (-\Delta H)V[\mathrm{X}][\mathrm{Y}]A\mathrm{e}^{-E/RT} - \chi S(T - T_{\mathrm{a}}) + \sigma 2k_{\mathrm{f}}'c_p(T_{\mathrm{a}} - T). \tag{3}$$

The first term on the right-hand side of (3) represents the heat generated by the reaction within the reactor. The second term represents the heat energy lost to the reactor's surrounding (in accordance with Newton's law of cooling with heat transfer coefficient χ). Finally, the last term on the right-hand side of equation (3) represents the net inflow of heat into the CSTR from the incoming reactants. We assume that the temperature of the fresh reactants is the same as the ambient (oven) temperature. We note that the term which represents the net inflow of heat into the CSTR has been multiplied by 2. This is due to the fact that our formulation has two feed streams into the CSTR, one

for each reactant. Such a formulation is important since if we would have only considered the one inflow pipe version, the reaction would commence in the inflow pipe rather than the reactor. In appendix A we discuss the reaction with two feed streams and show that it is equivalent to the one pipe version when appropriate rescaling is undertaken.

To assist the analysis of the model, dimensionless variables are normally introduced. Some forethought is required in the choice of dimensionless variables, as it is important that any physical parameters which are to be used as control variables retain their independence. (See [21,29,30] for further discussion regarding the importance of proper non-dimensionalisation. The former reference provides examples of how previous studies of reactions in CSTRs have been flawed due to improper non-dimensionalisation procedures.) In other words, the bifurcation parameters which are identified later on in this study must correspond explicitly to the experimental control parameters (that is, those parameters which the experimentalist can vary easily in the laboratory environment). According to Baulch et al. [23] and Di Maio et al. [31], the obvious experimental control parameters are: the composition of the input chemicals, the temperature of the oven in which the vessel is located (that is, the ambient temperature T_a), the flow rate k_f' (or equivalently, the residence time of the chemicals in the vessel which is given by $1/k_f'$), and the reactant pressure. In this study, we shall consider the first three as the bifurcation parameters. It follows that with this choice of bifurcation parameters, one method of non-dimensionalizing the governing equations (2) and (3) is to introduce the dimensionless temperature, time and concentrations of X and Y respectively as

$$u = \frac{RT}{E}, \qquad t = \frac{t'}{t_0}, \qquad x = \frac{[\mathrm{X}]}{[\mathrm{X}]_0 + [\mathrm{Y}]_0}, \qquad y = \frac{[\mathrm{Y}]}{[\mathrm{X}]_0 + [\mathrm{Y}]_0},$$

where $[\mathrm{X}]_0 + [\mathrm{Y}]_0 = C_0$. Here t_0 is some (unspecified) reference time, and C_0 is the fixed total concentration of the inflowing reactants. It follows that with this choice of non-dimensionalization the solution is dependent upon the following dimensionless quantities:

$$u_a = \frac{RT_a}{E}, \qquad k_f = \frac{k_f' t_0}{V}, \qquad \alpha = A\big([\mathrm{X}]_0 + [\mathrm{Y}]_0\big)t_0,$$

$$\ell = \frac{\chi S t_0}{\sigma V c_p}, \qquad \beta = \frac{(-\Delta H)R([\mathrm{X}]_0 + [\mathrm{Y}]_0)}{\sigma c_p E}.$$

The first of these parameters, u_a measures the oven temperature and the second parameter, k_f is the dimensionless flow rate. The quantity α is basically the dimensionless pre-exponential factor of the rate constant whereas ℓ is the coefficient of proportionality in the Newtonian cooling term. The dimensionless heat of the reaction is given by β.

In terms of these new non-dimensional quantities, the governing equations may be written as

$$\begin{aligned}
\frac{\mathrm{d}x}{\mathrm{d}t} &= k_{\mathrm{f}}(x_0 - 2x) - \alpha x y \mathrm{e}^{-1/u}, \\
\frac{\mathrm{d}y}{\mathrm{d}t} &= k_{\mathrm{f}}(y_0 - 2y) - \alpha x y \mathrm{e}^{-1/u}, \\
\frac{\mathrm{d}u}{\mathrm{d}t} &= \alpha\beta x y \mathrm{e}^{-1/u} - (2k_{\mathrm{f}} + \ell)(u - u_{\mathrm{a}}).
\end{aligned} \tag{4}$$

This model can be reduced to a two-dimensional system by subtracting the differential equations involving the concentrations and solving the resultant equation, and either specifying a special initial condition, that is the concentration of the reactants in the CSTR is the difference of the input concentrations, $x_0 - y_0$, or by considering $t \rightarrow \infty$. However, here we will consider the full three-dimensional model for the remainder of our investigation rather than the special two-dimensional case.

2.1. Existence of a region of ultimate confinement

For our present model we can show that there exists a region of ultimate confinement, in other words, the system has a finite attractor. This "trapping" result can be proven by referring to the governing equations (4) and deducing the following:

(i) Along $x = 0$, $\mathrm{d}x/\mathrm{d}t > 0$. Similarly along $y = 0$, $\mathrm{d}y/\mathrm{d}t > 0$.

(ii) For $x \geqslant x_0/2$, and for any values of y and u, $\mathrm{d}x/\mathrm{d}t < 0$. Similarly for $y \geqslant y_0/2$, and for any values of x and u, $\mathrm{d}y/\mathrm{d}t < 0$.
Hence, from (i) and (ii) both x and y are ultimately bounded.

(iii) For $0 \leqslant u \leqslant u_{\mathrm{a}}$, $\mathrm{d}u/\mathrm{d}t > 0$.

(iv) For sufficiently large u with x and y finite (since they have already been proven to be bounded), $\mathrm{d}u/\mathrm{d}t \rightarrow -(2k_{\mathrm{f}} + \ell)u < 0$. Hence, u is also ultimately bounded.

We have, therefore, demonstrated the existence of a globally attracting invariant region for the scheme (4) in the CSTR. As a consequence, once the trajectories enter this region of the phase space, it cannot emerge from its boundaries.

3. Steady states

The steady states $(x_{\mathrm{s}}, y_{\mathrm{s}}, u_{\mathrm{s}})$ of the model are determined by setting the three time derivatives in (4) to zero. By combining these equations, the steady state concentration x_{s} can be shown to be the (positive) solution of the following quadratic equation:

$$\alpha \mathrm{e}^{1/u_{\mathrm{s}}}(x_{\mathrm{s}})^2 + \left(2k_{\mathrm{f}} - x_0\alpha\mathrm{e}^{1/u_{\mathrm{s}}} + \frac{1}{2}\alpha\mathrm{e}^{1/u_{\mathrm{s}}}\right)x_{\mathrm{s}} - k_{\mathrm{f}}x_0 = 0, \tag{5}$$

with the equilibrium concentration y_s given by

$$y_s = x_s - x_0 + \frac{1}{2}. \tag{6}$$

It is clear from the above equations that x_s and y_s are expressed in terms of the steady state temperature u_s. Hence, u_s is found to be the root of the transcendental equation

$$\alpha\beta x_s y_s e^{1/u_s} = (2k_f + \ell)(u_s - u_a). \tag{7}$$

The stability of the above steady state solutions can be determined by the usual way of linearizing about the stationary values of x_s, y_s and u_s (see [32]). This is found to involve the growth function $e^{\lambda t}$, where the (complex) constant λ is given by the eigenvalues of the following 3×3 Jacobian matrix:

$$J = \begin{pmatrix} J_A & J_B & J_C \\ J_D & J_E & J_F \\ J_G & J_H & J_I \end{pmatrix} \tag{8}$$

where $J_A, \ldots, J_I$ are the appropriate partial derivatives (evaluated at the steady states) of the right-hand side of the governing equations (4). The characteristic polynomial for the eigenvalues can be shown to be

$$\lambda^3 + \widehat{b}\lambda^2 + \widehat{c}\,\lambda + \widehat{d} = 0, \tag{9}$$

where

$$\begin{aligned} \widehat{b} &= -(J_A + J_E + J_I), \\ \widehat{c} &= J_A J_E + J_A J_I + J_E J_I - J_B J_D - J_C J_G - J_F J_H, \\ \widehat{d} &= -J_A J_E J_I - J_D J_C J_H - J_G J_B J_F + J_A J_F J_H + J_E J_G J_C - J_I J_B J_D. \end{aligned}$$

When applying the generalized Hopf theorem to our system (see [32]), we require one of the eigenvalues to be negative and the other two to be purely imaginary. Hence, for the Hopf condition to be satisfied (following [3]), we require the cubic equation (9) to be written in the form

$$\left(\lambda^2 + \omega_n^2\right)\left(\lambda + \widehat{a}\right) = 0, \quad \widehat{a} > 0.$$

By comparing these cubic equations in λ, we obtain the Hopf conditions for our system. These conditions can be expressed as

$$\widehat{b}\widehat{c} - \widehat{d} = 0, \quad \widehat{b},\ \widehat{c},\ \widehat{d} > 0. \tag{10}$$

The corresponding period of oscillations at the Hopf point is given by

$$P = \frac{2\pi}{\sqrt{\widehat{c}}}. \tag{11}$$

Hence, parameter values that result in the condition (10) to be satisfied are the points in the parameter space at which oscillatory solutions are generated from the steady state solutions.

The boundary separating the regions containing one and three steady state solutions (that is, the change over from one and three equilibria), often referred to as the saddle-node bifurcation point locus, occur when one of the eigenvalues of the Jacobian matrix (8) becomes zero. This condition is satisfied when

$$\widehat{d} = 0, \tag{12}$$

that is, whenever the determinant of the Jacobian matrix becomes zero.

The locations of both the Hopf and saddle-node loci have been sketched in the (x_0, u_a), (x_0, k_f) and (u_a, k_f) parameter planes, and are presented in section 4. We have decided to display these plots in several two-dimensional plots rather than a three-dimensional surface in the (x_0, u_a, k_f) parameter plane because we have found that the latter does not display the dynamical results particularly well as several important features are obscured by the surface plot (despite our attempts to orientate the surface).

4. Results of numerical computation

In this section, we present and analyse the results of numerical computation, with the aim of providing a description of the global structure of the solutions to the model (4). The path following software AUTO97 [33] was used to obtain both the steady state and the periodic solutions. We also utilised the Maple software program in conjunction with AUTO97 to obtain accurate location of the Hopf and saddle-node loci in the parameter space. The dimensionless quantities $\alpha = 5.0$ and $\beta = 1.7$ (which represent the pre-exponential factor and the heat of the reaction, respectively), were fixed throughout the course of our investigation. In sections 4.1–4.3 we present results of our investigation of the behaviour of the system in the control parameter space (i.e., the input concentration–ambient temperature–flow rate parameter space).

4.1. The (x_0, u_a) parameter space

We will begin our investigation of the system (4) by studying both the Hopf and saddle-node loci in the input concentration–ambient temperature parameter space. This is shown in figure 1(a) (with one value of heat loss parameter ℓ) and in figure 1(b) (displaying three values of ℓ). It is not surprising that the loci in these figures are symmetrical about $x_0 = 0.5$ since $x_0 + y_0 = 1$ (from our choice of non-dimensionalisation) and the choice of x or y as the fuel/oxidant is arbitrary. A close study of these figures shows that the Hopf curve and the saddle-node bifurcation line do not intersect at the cusp points as the figure might suggest (see enlarged view of the boxed region in figure 1(a)). The point where the Hopf curve meets the saddle-node bifurcation line is the the double-zero eigenvalue (DZE) degeneracy, often referred to as the Bogdanov–Takens bifurcation. Figures 1(a) and (b) clearly show two double-zero eigenvalue points

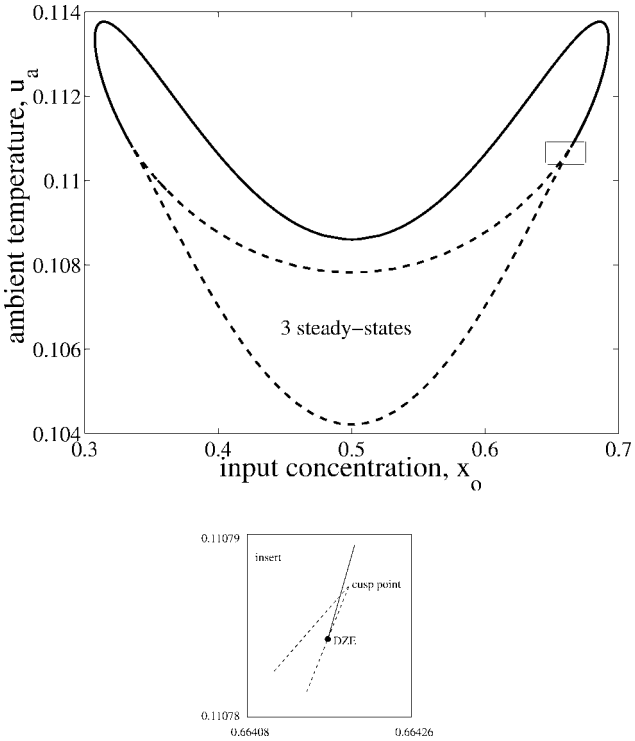

(a)

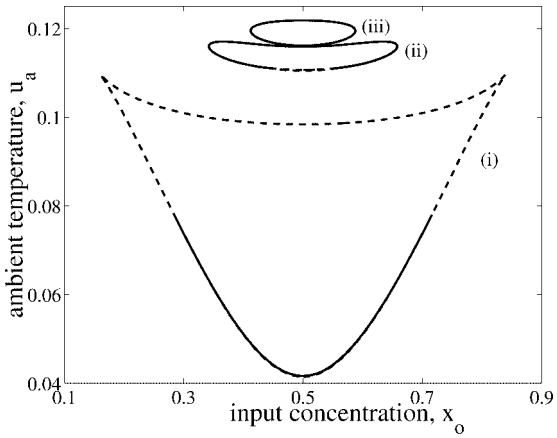

(b)

Figure 1. (a) The location of the Hopf curve (solid line) and the border between regions possessing one and three equilibria (dashed curve) in the (x_0, u_a) parameter plane. Results are shown for flow rate $k_f = 1.6 \times 10^{-3}$ and heat loss coefficient $\ell = 5 \times 10^{-3}$ with an enlarged view of the boxed region displaying the location of the double-zero eigenvalue (DZE) degeneracy point. (b) The location of the Hopf locus (solid line) and the saddle-node curve (dashed curve) in the (x_0, u_a) parameter plane. Results are shown for $k_f = 1.6 \times 10^{-3}$ with (i) $\ell = 1.5 \times 10^{-3}$, (ii) $\ell = 6 \times 10^{-3}$ and (iii) $\ell = 7.5 \times 10^{-3}$.

in most cases (except when $\ell = 7.5 \times 10^{-3}$ where there are no double-zero eigenvalues since there are no limit points in this case), one at each end of the Hopf curve. The main importance of double-zero eigenvalue points is that these points give rise to the appearance of a homoclinic orbit for nearby parameter values (see [34]). Such homoclinic orbits have been observed experimentally for the oxidation of acetaldehyde in the CSTR [35] and in the detailed mathematical analysis undertaken by Gray and Forbes [36] and Sidhu et al. [37].

During our investigation of varying the heat loss parameter ℓ, it was observed that the Hopf points existed over the range $1.025802 \times 10^{-3} \leqslant \ell \leqslant 8.199308 \times 10^{-3}$, while the multiple steady state solutions were only possible for $0 \leqslant \ell \leqslant 6.176921 \times 10^{-3}$ (where $\ell = 0$ is the adiabatic limit). This shows that multiplicity is not a prerequisite for oscillatory behaviour (see [38] for further examples). It was also seen that as ℓ was increased from 0, the DZE points appear on the lower branch of the saddle-node curve at $x_0 = 0.5$ when $\ell = 1.025802 \times 10^{-3}$ and proceed to move along the saddle node curve. Here we note that initially the saddle-node locus and the Hopf curve in this parameter plane was difficult to distinguish (see, for example, the loci for these points for $\ell = 1.5 \times 10^{-3}$ in figure 1(b)). As the heat loss parameter was increased, the DZE points moved through the cusp points and onto the upper branch. It is also important to note that as ℓ is increased, the region of multiple stationary state solutions reduces which can be observed in figure 1(b). Finally, at $\ell = 6.176921 \times 10^{-3}$, the DZE points coalesce at $x_0 = 0.5$, and for $\ell > 6.176921 \times 10^{-3}$, the Hopf curve becomes a closed loop, with no multiple steady state solutions (for example, see figure 1(b) with $\ell = 7.5 \times 10^{-3}$).

Next we investigate the system by fixing input concentration x_0 (which in effect fixes the ratio of the input mixture of chemicals X and Y), and varying the ambient (oven) temperature u_a. This is equivalent to taking vertical cuts through figure 1(a). As mentioned earlier, the curves in figures 1(a) and (b) are symmetrical about $x_0 = 0.5$, therefore, the dynamical behaviour of the system is exactly the same if x_0 is either increased or decreased from $x_0 = 0.5$. As a result, we will only consider the behaviour of the system as the control parameter x_0 is increased. The steady-state diagrams in figures 2(a) and (b) display the behaviour of the system (4) as the ambient temperature is varied for the two cases of input concentrations $x_0 = 0.5$, and $x_0 = 0.68$, respectively. These values were chosen since they correspond to the value of x_0 on either side of the Bogdanov–Takens bifurcation (DZE) point.

Figure 2(a) shows the steady state temperature u_s as a function of the ambient temperature u_a for $x_0 = 0.5$ (that is, when species X and Y are pumped into the CSTR at stoichiometry, i.e., in the ratio 1 : 1). We can see the region in which multiple steady state solutions are possible (between the two saddle-node bifurcation points denoted LP1 and LP2 in the figure). This region of multiplicity can also be observed by considering a vertical line through the saddle-node curve (dashed line) in figure 1(a) at the value $x_0 = 0.5$. It is also evident from figure 1(a) that there is only one Hopf point associated with these parameter values. Furthermore, this Hopf point, which is located in the region where only a single equilibrium solution is possible and is labelled H1 in figure 2(a), is

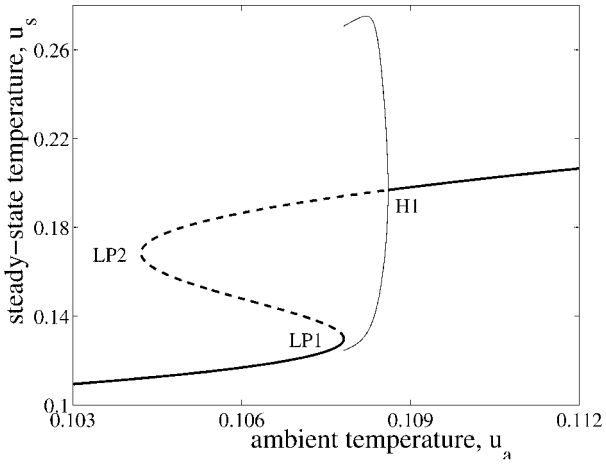

(a)

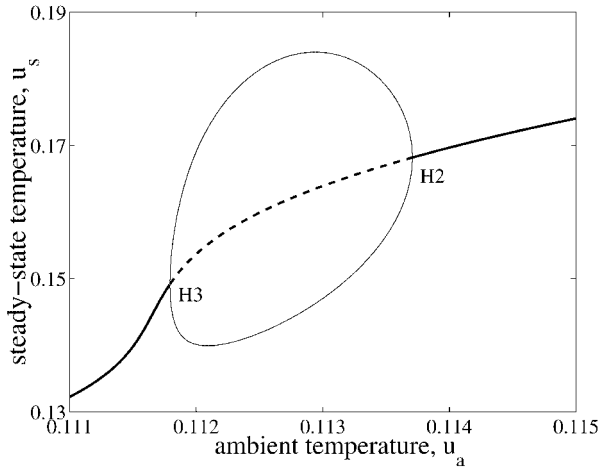

(b)

Figure 2. The dependence of steady-state temperature u_s upon ambient temperature u_a for $k_f = 1.6 \times 10^{-3}$, $\ell = 5 \times 10^{-3}$, (a) $x_0 = 0.5$ and (b) $x_0 = 0.68$. Solid lines indicate stable equilibria and dashed lines denote unstable equilibria. The points labelled LP1 and LP2 represent the limit points (saddle-node bifurcation points) whereas the Hopf points are denoted by H1–H3. The stable periodic solution branch is denoted by the vertical line emerging from the Hopf points (the upper curve representing the maximum temperature attained during periodic oscillations, whereas the minimum temperatures are given by the lower branch).

associated with a supercritical Hopf bifurcation since a stable branch of periodic solutions emanates from this point.

As the ambient temperature is reduced from its value at the Hopf point, the amplitude of oscillations increases as seen in figure 2(a). It was also noticed that the fre-

quency of oscillations decreases (that is, the period of oscillations increases). Similar behaviour has been observed experimentally, for example, for the $H_2 + O_2$ reaction in the CSTR [23] and also the $H_2 + Cl_2$ reaction in the semibatch reactor [39]. As the ambient temperature is further reduced, the amplitude of oscillations reaches a maximum and begins to decrease, while the period of oscillations continues to increase. We were able to follow the periodic solution branch until the u_a value just below the corresponding value at the saddle-node point LP1 where it became difficult to continue numerically. A sharp, almost vertical, rise in the period of oscillations was noticed close to this value of ambient temperature. On closer examination of the phase plane at this point, it was found that this behaviour corresponds to a homoclinic destruction of the stable limit cycle with a saddle point close to this value of the ambient temperature. Hence, we have the situation in which a saddle-node bifurcation occurred at the value of u_a which corresponds to the value at LP1. As the value of u_a is further reduced, the saddle point and the stable node (both born from the saddle-node bifurcation point LP1), move apart, with the saddle point moving towards the limit cycle. It is the collision between the saddle point and the limit cycle that causes the homoclinic destruction of the limit cycle. It must be noted that all the above description occurs in a very narrow region of the ambient temperature, and would therefore be unlikely to be observed experimentally. In experiments one would basically conclude that as the ambient temperature is reduced, the oscillations would cease at the limit point LP1.

The point $(x_0, u_a) = (0.664158, 0.110787)$ in figure 1(a) is associated with the double-zero eigenvalue degeneracy. For x_0 greater than this value, there is an increase in the number of Hopf points from one to two. The lower Hopf bifurcation point is initially (for $0.664158 < x_0 < 0.664213$) located in a very narrow region of three equilibrium points, whereas the upper Hopf point lies in the region where only one equilibrium solution is possible. Furthermore, the upper Hopf bifurcation point is supercritical, behaving in a manner similar to the Hopf point H1 described in figure 2(a). The lower Hopf point, on the other hand, is initially associated with a subcritical Hopf bifurcation, and as a result, an unstable branch of periodic solutions emerges from this point which is destroyed via a homoclinic bifurcation.

As x_0 is increased further, figure 1(a) shows that both of the Hopf points lie in the region containing one equilibrium solution. Here, we observe the classical case where a periodic solution branch emerges from one Hopf point and terminates at the other when the ambient temperature is varied. This type of behaviour is illustrated in figure 2(b) (with $x_0 = 0.68$). As the input concentration x_0 is further increased, the Hopf points (H2 and H3 in figure 2(b)) begin to move closer together along the steady state solution branch, until finally they coalesce at $(x_0, u_a) = (0.692377, 0.113353)$. This point is sometimes referred to as the double Hopf bifurcation point or the $H2_1$ degenerate point (see [40]). For $x_0 > 0.692377$ (with heat loss coefficient $\ell = 5 \times 10^{-3}$ and flow rate $k_f = 1.6 \times 10^{-3}$), the periodic behaviour ceases to exist and a single (stable) equilibrium configuration exists.

4.2. The (u_a, k_f) parameter space

Figures 3 and 4 show the Hopf and saddle-node loci in the the ambient temperature–flow rate parameter space for three different values of input concentration x_0. Figure 3(a) (with $x_0 = 0.5$) shows a large region where multiple steady state solutions are possible, and the Hopf curve (bold curve) appearing at the lower part of the saddle-node locus. Figure 3(b) displays the enlargement of this region showing the two Bogdanov–Takens bifurcation points (DZE1 and DZE2) at which the Hopf curve terminates when it intersects with the saddle-node curve, while figure 3(c) shows clearly the location of the DZE2 point in relation to the cusp point in the saddle-node locus. Figure 3(b) shows close resemblance to the minimal bromate system's "cross-shaped" diagram as described by Gray and Scott [3, pp. 400–402]. Figure 4 shows that as the input concentration x_0 increases (or alternatively, input concentration y_0 decreases), the region of multiple steady state solution decreases until finally for $x_0 > 0.744987$, the system only exhibits one stationary state solution. Similarly the oscillatory solutions cease for $x_0 > 0.693997$ which one would expect given the structure of the curves in figure 1.

From figure 3(a) (with $x_0 = 0.5$) we can see that for $k_f > 0.024623$ (i.e., for values of flow rate larger than the upper cusp point) multiple steady state solutions are not possible. As k_f is reduced to values between this upper cusp point and the value of k_f at the DZE1 point (i.e., $3.6156 \times 10^{-3} < k_f < 2.4623 \times 10^{-2}$) we obtain steady-state diagrams that resemble the classical ignition–extinction diagrams (see, for example, figure 5(a) with $k_f = 0.01$).

For values of flow rates between the DZE1 and the point marked HSN (the non-local cross-over of the Hopf locus and the saddle-node curve) on figure 3(b), i.e., $1.6481 \times 10^{-3} < k_f < 3.6156 \times 10^{-3}$, there exists a single Hopf point which is located in the region of three stationary state solutions. Furthermore, these Hopf points are associated with subcritical Hopf bifurcation and unstable periodic solution branches emanate from these points. Figure 5(b) (with $k_f = 2.0 \times 10^{-3}$) shows a typical behaviour of the system in this range of flow rates. The steady-state diagram shows that the unstable limit cycles increase in size as the ambient temperature u_a is increased until it undergoes a homoclinic destruction at the saddle point. For values of flow rates below the HSN point (from figure 3(b)), the system's behaviour is similar to that discussed in the previous section and as such these results will only be summarized below.

For values of flow rates between the HSN point and the double-zero eigenvalue point DZE2 (see figures 3(b) and (c)), we obtain steady-state diagrams very similar to figure 2(a) (stable periodic solutions emerging from the single supercritical Hopf point located in a single steady state configuration, and as the ambient temperature is decreased, this periodic solution branch ceases close to the saddle-node bifurcation point via a homoclinic bifurcation). For values of k_f below the the DZE2 point, the number of Hopf bifurcation points increases to two; the lower being initially subcritical whereas the upper is supercritical. As the flow rate is further decreased below the lower cusp point of

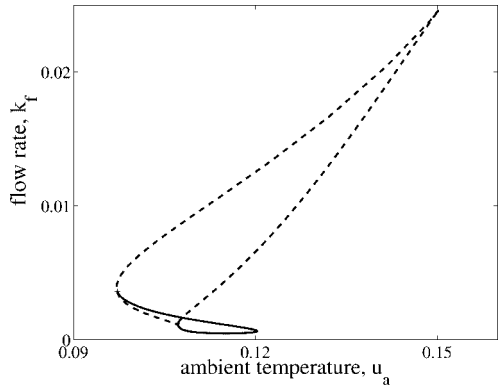

(a)

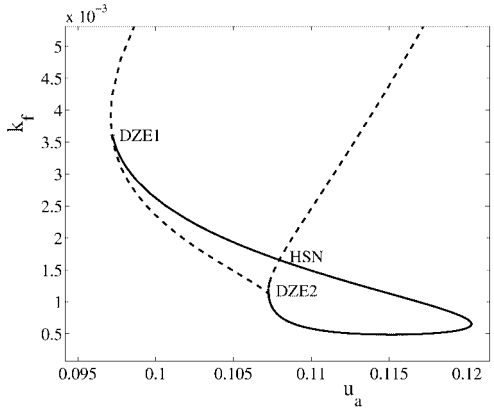

(b)

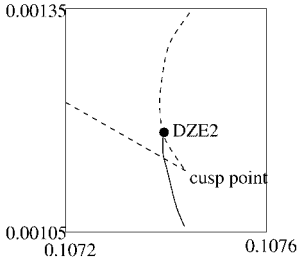

(c)

Figure 3. (a) The location of the Hopf locus (solid line) and the saddle-node curve (dashed curve) in the (u_a, k_f) parameter plane with stoichiometric input concentrations, i.e., $x_0 = y_0 = 0.5$. (b) Enlarged view of the Hopf curve in (a), showing the locations of the two double-zero eigenvalue points (DZE1 and DZE2) and the non-local crossing of the Hopf curve with the saddle-node curve (labelled HSN). (c) Enlarged view of the region around DZE2.

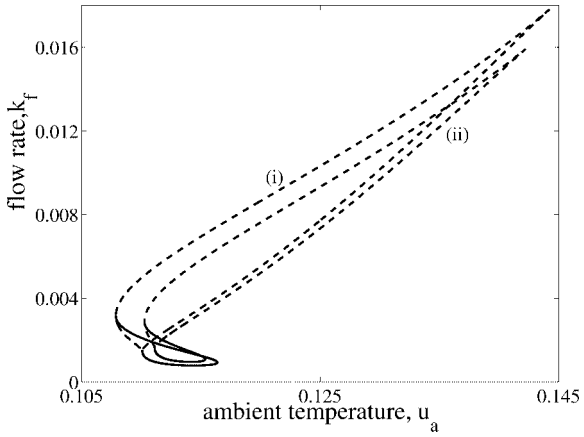

Figure 4. The location of the Hopf locus (solid line) and the saddle-node curve (dashed curve) in the (u_a, k_f) parameter plane with two values of input concentrations: (i) $x_0 = 0.65$ and (ii) $x_0 = 0.67$.

the saddle-node locus, we observe the classical case whereby periodic solutions emerge from one Hopf point and terminate at the other when the ambient temperature is varied (similar to figure 2(b)). Since we are below the lower cusp point, the two Hopf points are associated with single steady-state configuration. This type of behaviour persists until k_f reaches the minimum value on the Hopf locus (the double Hopf bifurcation point or the $H2_1$ degenerate point) after which further reduction in the flow rate results in a single stable steady-state configuration.

4.3. The (x_0, k_f) parameter space

Figure 6 shows the regions of multiple steady-state solutions (dashed line) and the Hopf bifurcation points (bold line) for two values of ambient temperatures $u_a = 0.114$ and $u_a = 0.105$. These values of ambient temperature were chosen to represent two different cases from figure 3 (the former for u_a in which two Hopf point were present in single steady state configuration, and the latter to represent a single Hopf point located in a region of multiple equilibria).

For ambient temperature $u_a = 0.114$, figure 6 shows that the saddle-node and Hopf loci are separate from each other. We reiterate that these loci are symmetrical about $x_0 = 0.5$ for reasons that already have been discussed. As the ambient temperature is reduced, the saddle-node and Hopf loci not only move closer to each other, but shrink in size as well. As the ambient temperature is reduced past the value at the Bogdanov–Takens bifurcation point DZE2 in figure 3(b), the lower Hopf bifurcation branch disappears resulting in in only the upper Hopf loci which exists within the region of multiple steady-state solutions. Here we note that the upper Hopf locus crosses the saddle-node locus non-locally and as a result it is not destroyed during this process,

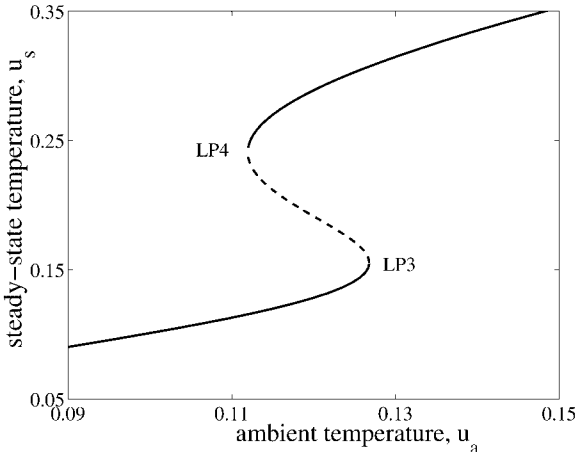

(a)

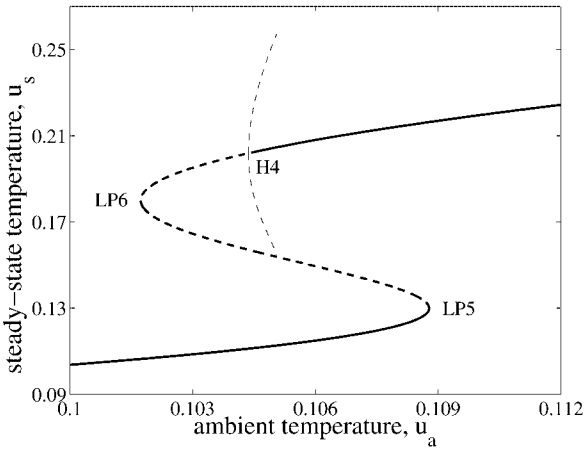

(b)

Figure 5. The steady-state curve of the system as the ambient temperature u_a is varied with the concentrations of the reactants at the inflow fixed at stoichiometric values. The flow rates are (a) $k_f = 0.01$, and (b) $k_f = 0.002$. The limit points are labelled LP3–LP6, while H4 is a subcritical Hopf bifurcation point. The vertical dashed line emerging from H4 denotes the unstable periodic solution branch. The rest of the notation is similar to figure 2.

but this is not the case for the lower Hopf curve. This is obvious from figure 6 with $u_a = 0.105$.

As u_a is decreased even further, the two DZE points that appear in figure 6, begin to move closer to each other (in other words, the Hopf curve is reducing in size), until they finally coalesce at $x_0 = 0.5$ at the value of u_a which corresponds to the value of

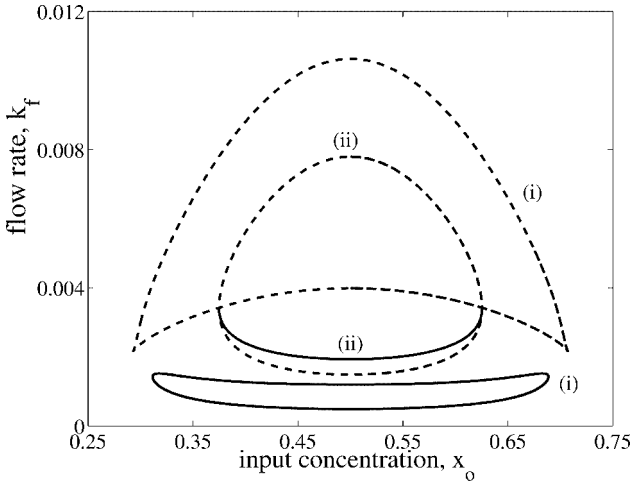

Figure 6. The location of the Hopf locus (solid line) and the saddle-node curve (dashed curve) in the (x_0, k_f) parameter plane. Results are shown with the ambient temperature fixed at (i) $u_a = 0.114$ and (ii) $u_a = 0.105$.

the DZE1 point in figure 3(b) (i.e., $u_a = 0.097218$). The region of multiple equilibria which in the meantime is also shrinking as u_a is decreased, and disappears soon after the possibility of oscillations ceases.

Figure 7 shows the dependence of equilibrium temperature u_s upon the flow rate k_f for the two values of ambient temperatures mentioned previously (with the input concentrations of chemicals X and Y kept at the ratio 1 : 1). Figure 7(a) contains a single hysteresis loop with two supercritical Hopf points located at low flow rates. As the ambient temperature is reduced further, a steady-state diagram resembling a mushroom is observed (which persists only for a narrow band of ambient temperature). Further reduction in the ambient temperature results in the formation of an isola which is shown in figure 7(b). It is interesting to note that the isola formed here has not done so in the usual way (through a mushroom first, and then having two limit points coalescing as a bifurcation parameter is varied resulting in the steady-state curve "pinching off" causing the presence of two disjoint branches, see [3] for examples). In this case, as the ambient temperature is reduced, the limit point LP7 and the lower Hopf point H5 (in figure 5(a)) move closer to each other and finally coalesce which results in the isola. This Hopf bifurcation point is destroyed in this process and as a result only one Hopf point exists and is located on the isola as shown in figure 5(b). In addition, this Hopf point is subcritical with an unstable periodic solution branch which emanates from it is terminated via a homoclinic bifurcation at a saddle point. This isola reduces in size when the ambient temperature is reduced, and finally the whole isola disappears leaving only the lower stable steady state solution branch as the ambient temperature is reduced further.

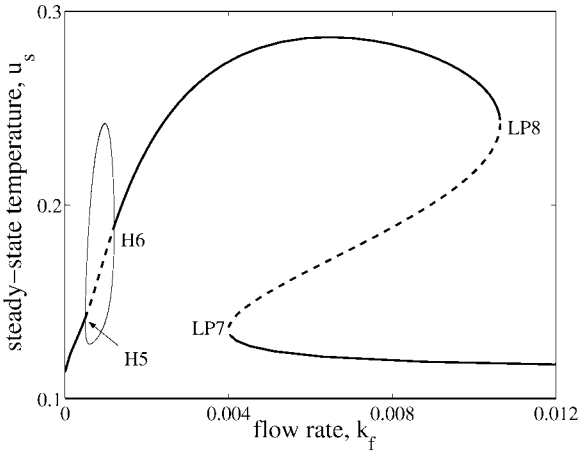

(a)

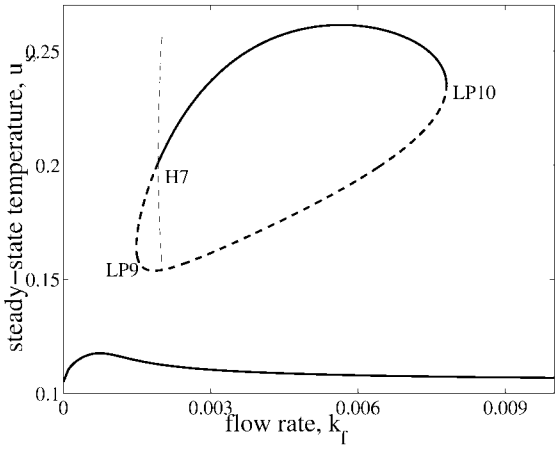

(b)

Figure 7. The dependence of steady-state temperature u_s upon flow rate k_f with the concentrations of the reactants at the inflow maintained at stoichiometry. The ambient temperature is (a) $u_a = 0.114$ and (b) $u_a = 0.105$. The limit points are LP7–LP10, while the Hopf bifurcation points are H5–H7. The vertical dashed line emerging from the Hopf points denotes the periodic solution branches; stable and unstable periodic solution branches are denoted by solid and dashed lines, respectively. The rest of the notation is similar to figure 2.

5. Flammability limits

In this section we undertake a preliminary study of how the bifurcation diagram, figure 6, can be used to map out regions where the mixture of fuel–oxygen can be considered as flammable. This figure, a bifurcation diagram showing regions where the limit

point and Hopf loci are located in the flowrate–input concentration parameter plane, was chosen because flammability experiments correspond to fixing the ambient temperature and varying the fuel fraction.

When the oven temperature is fixed at $u_a = 0.105$ (curves (ii) in figure 6), we investigate three cases of different flow rates which represent three important regions in the bifurcation diagram. We study the behaviour of the fuel–oxygen mixture using the concentration of fuel at the input, x_0, as the continuation parameter. Here we have assumed that the input concentration x_0 represents the input concentration of the fuel, however, the choice of x or y being the fuel or oxygen species is not significant as the governing equations (4) are symmetric in x and y.

Figure 8(a) shows two disjoint steady-state solution branches; a stable lower branch (no-ignition branch) and an isola which contains stable and unstable solution branches. The stability of the isola changes at the two limit points LP11 and LP12, which can be characterised as the extinction points of the system. The fuel–oxygen mixture is flammable only if the composition of the input concentration lies between the values of x_0 at LP11 (fuel-lean limit) and LP12 (the fuel-rich limit). An important point to note here is that there is no ignition point in this case. Hence, an appropriate initial condition for temperature (a sufficiently strong ignition source) is required within the fuel-lean and fuel-rich limits to ignite the mixture (that is, to attain the upper, "hot" stable steady-state solution branch). Here ignition does *not* occur by the gradual increase of the fuel concentration which can be hazardous.

When the flow rate is lowered to $k_f = 0.0025$, we can see from figure 6 that we are now in a region where two Hopf points exists. Figure 8(b) shows these Hopf points (which are both subcritical) and an important feature is that the stability no longer changes at the limit points, but does so at the two Hopf points, H8 and H9. Therefore, the latter two points now define to the fuel-lean and fuel-rich flammability limts. In this case the locus of the Hopf points plays an important role in determining the flammability limits which unlike the previous case were determined only by the saddle-node bifurcation points. The role of the Hopf locus in determining the flammability limits is interesting as the investigation of Spalding [41] focussed only on the extinction limits points on the isola.

As the flow rate is reduced further, the size of the isola decreases and at the same time, the two subcritical Hopf points (H8 and H9 in figure 8(b)) move close together and finally coalesce at the value of the flow rate k_f which corresponds to the double Hopf bifurcation point (the minimum value of the flow rate on the Hopf locus in figure 6). Below this value of k_f there are *no* stable solution branch on the isola (see figure 8(c) for $k_f = 0.0015$). Since there is no upper stable solution branch, the "hot" state does not exist and for these cases, regardless of the value of the ignition source, the mixture cannot ignite, and therefore, the mixture is never flammable.

By assembling all the information that we have discussed in this section, one can map out the regions of the bifurcation diagram in which the mixture is and is not flammable for a fixed ambient temperature. This is shown in figure 9. As mentioned earlier, the study presented here is only a preliminary investigation of flammability limits of our

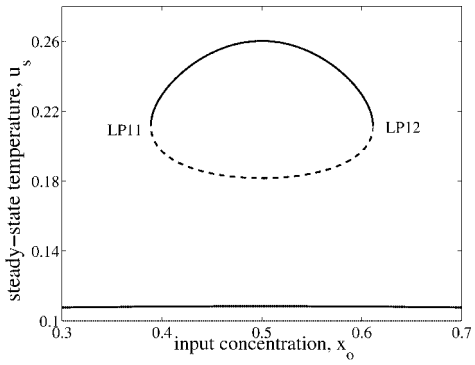

(a)

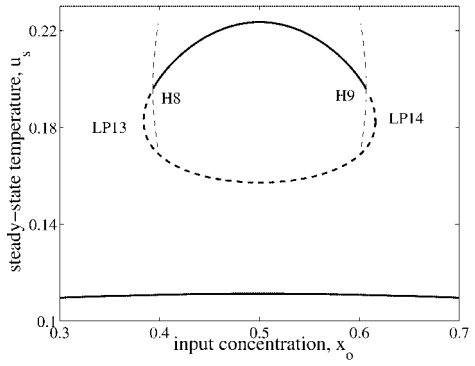

(b)

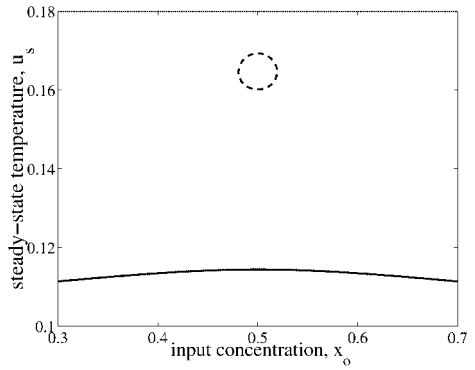

(c)

Figure 8. The steady-state diagrams with ambient temperature fixed at $u_a = 0.105$ and the flow rates (a) $k_f = 0.005$, (b) $k_f = 0.0025$ and (c) $k_f = 0.0015$. The limit points and Hopf bifurcation points are labelled as before, and the unstable periodic solution branch emerging from the Hopf points is denoted by the vertical dashed line.

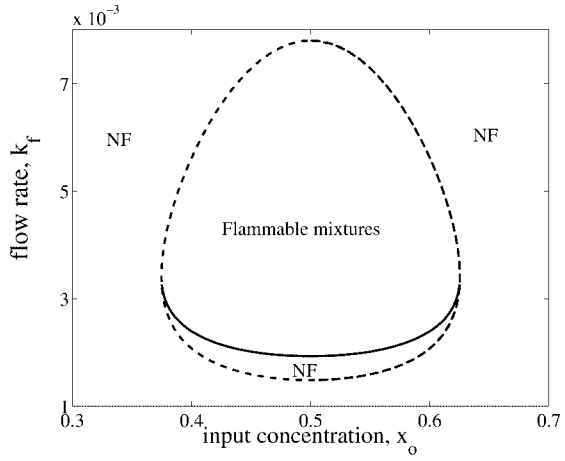

Figure 9. The variation of the flammability limits of the fuel–oxygen mixture as a function of the flow rate for the case when the ambient temperature is fixed at $u_a = 0.105$. The abbreviation NF refers to non-flammable mixture.

scheme in the CSTR. A detailed investigation of the flammability limits in a oxygen–fuel–inert mixture in a CSTR will be presented in [26].

6. Conclusions

In this paper we have undertaken a mathematical analysis of a single step second order exothermic reaction in a CSTR. The non-dimensionalised variables used were chosen to ensure that the experimentally controllable parameters retained their independence. We studied the response of the system to changes in the ambient temperature, the flow rate and the input concentration. These parameters were chosen because they are easily varied between or during experiments. We also investigated the effect of heat losses. Although the latter is not easily changed in a given experiment setup, it is still an important reactor design parameter (Ball and Gray [21]).

The results of our investigation have shown that this simple system exhibits a wide range of nonlinear behaviour ranging from multiplicity to stable and unstable periodic solutions. We have shown that the Hopf points can be either subcritical or supercritical, depending upon parameters. A particularly interesting feature of this system is that the flammability limits may be defined by Hopf bifurcation points on an isola rather than limits points, as is usually thought to be the case. From the associated locus of the bifurcation points it is then possible to determine which parts of parameter space define flammable mixtures.

Since this is only a preliminary investigation we have only undertaken a co-dimension 0 singularity analysis, a higher co-dimension investigation is currently being undertaken.

Acknowledgement

The authors are very grateful to Professor B.F. Gray for his helpful discussions. M.I.N. is supported by a grant by the Australian Research Council.

Appendix A. Equivalence of multi-pipe CSTRs and the one-pipe version

The governing equations (4) for a two-pipe inflow CSTR can be easily shown to transform to the following differential equations:

$$\begin{aligned}
\frac{\mathrm{d}x}{\mathrm{d}t} &= k_{\mathrm{f}}^{*}\left(x_0^{*} - x\right) - \alpha x y \mathrm{e}^{-1/u}, \\
\frac{\mathrm{d}y}{\mathrm{d}t} &= k_{\mathrm{f}}^{*}\left(y_0^{*} - y\right) - \alpha x y \mathrm{e}^{-1/u}, \\
\frac{\mathrm{d}u}{\mathrm{d}t} &= \alpha\beta x y \mathrm{e}^{-1/u} - \left(k_{\mathrm{f}}^{*} + \ell\right)(u - u_{\mathrm{a}}),
\end{aligned} \tag{A.1}$$

simply by rescaling the flow rate and input concentrations as

$$k_{\mathrm{f}}^{*} = 2k_{\mathrm{f}}, \qquad x_0^{*} = \frac{x_0}{2}, \qquad y_0^{*} = \frac{y_0}{2}. \tag{A.2}$$

We now consider two cases related to these equations:

1. The set of equations given in (A.1) appear to describe the scenario of the reaction (1) if it was occurring in the one-pipe CSTR. One may immediately imagine that the experimental setting which is described by these equations appear to be that of the mixture X + Y being pumped into the inflow pipe. Obviously, such an experimental scenario is not very satisfactory since it leads to the possibility of the reaction occuring in the inflow pipe rather than in the reactor.
2. If the equations in (A.1) were written down to describe reaction (1) in a two-pipe CSTR, at first-sight it appears that the whole modelling process has gone terribly wrong. Equations (A.1) appear to suggest that there is a mismatch in the inflow and outflow rates (that is, if there are two feed streams into the reactor with each flow rate being k_{f}^{*}, then the volumetric flow rate out of the reactor must be $2k_{\mathrm{f}}^{*}$, and not k_{f}^{*} which these equations seem to suggest) which indicates immediately that the dynamical equation for $\mathrm{d}V/\mathrm{d}t$ (rate of change of volume) must be included in the governing equations as well.

In both of the above cases, we can see why results obtained from the set of equations given in (A.1) to describe the reaction (1) could be dismissed if the scaling process (A.2) is not explicitly made clear. The original equations (4) have the obvious advantage of being related directly to experimental parameters and therefore have been considered in the investigation presented in this paper. However, the results obtained from the system (A.1) can still be valid and should not be disregarded. Furthermore, given the results and analysis for a one-pipe CSTR, we can easily use a scaling process

similar to (A.2) to obtain the corresponding results for a multi-pipe CSTR without actually having to rework the analysis (as long as the scaling process does not yield results which are unphysical).

Appendix B. Nomenclature

A	pre-exponential factor ($m^3\ mol^{-1}\ s^{-1}$)
E	activation energy ($J\ mol^{-1}$)
R	gas constant ($J\ mol^{-1}\ K^{-1}$)
T	reactant temperature (K)
T_a	temperature of the oven (K)
V	volume of CSTR (m^3)
[X], [Y]	reactant concentrations ($mol\ m^{-3}$)
$[X]_0$, $[Y]_0$	reactant concentrations at inflow ($mol\ m^{-3}$)
c_p	molar heat capacity of reactants at constant pressure ($J\ mol^{-1}\ K^{-1}$)
ℓ	dimensionless surface heat transfer coefficient $= \chi S t_0/(\sigma V c_p)$
k_f'	volume flow rate ($m^3\ s^{-1}$)
k_f	dimensionless flow rate $= k_f' t_0/V$
t	dimensionless time $= t/t_0$
t'	time (s)
t_0	some unspecified reference time (s)
u	dimensionless temperature of the reaction $= RT/E$
u_a	dimensionless ambient temperature $= RT_a/E$
x	dimensionless concentration of chemical X $= [X]/([X]_0 + [Y]_0)$
y	dimensionless concentration of chemical Y $= [Y]/([X]_0 + [Y]_0)$
α	dimensionless pre-exponential factor $= A([X]_0 + [Y]_0)t_0$
β	dimensionless molar enthalpy change $= ([X]_0 + [Y]_0)(-\Delta H)R/(\sigma c_p E)$
χ	surface heat transfer coefficient ($W\ m^{-2}\ K^{-1}$)
ΔH	molar enthalpy change ($J\ mol^{-1}$)
σ	molar density ($mol\ m^{-3}$)

References

[1] I.R. Epstein and J.A. Pojman, *An Introduction to Nonlinear Chemical Dynamics* (Oxford University Press, New York, 1998).
[2] R.J. Field and M. Burger, *Oscillations and Travelling Waves in Chemical Systems* (Wiley, New York, 1985).
[3] P. Gray and S.K. Scott, *Chemical Oscillations and Instabilities* (Clarendon Press, Oxford, 1994).
[4] Ya.B. Zeldovich, I. Zh. Tekh. Fiz. 11 (1941) 493.
[5] C. van Heerden, Ind. Engrg. Chem. 45 (1953) 1242.
[6] O. Bilous and N.R. Amundson, AIChE J. 1 (1955) 513.
[7] R. Aris and N.R. Amundson, Chem. Engrg. Sci. 7 (1958) 121.
[8] R. Aris and N.R. Amundson, Chem. Engrg. Sci. 7 (1958) 132.
[9] R. Aris and N.R. Amundson, Chem. Engrg. Sci. 7 (1958) 148.
[10] V. Hlavacek, M. Kubicek and J. Jelinek, Chem. Engrg. Sci. 25 (1970) 1441.
[11] A. Uppal, W.H. Ray and A.B. Poore, Chem. Engrg. Sci. 29 (1974) 967.
[12] A. Uppal, W.H. Ray and A.B. Poore, Chem. Engrg. Sci. 31 (1976) 205.
[13] V. Balakotaiah and D. Luss, Chem. Engrg. Commun. 13 (1981) 111.
[14] V. Balakotaiah and D. Luss, Chem. Engrg. Commun. 19 (1982) 185.
[15] V. Balakotaiah and D. Luss, Chem. Engrg. Sci. 37 (1982) 433.
[16] V. Balakotaiah and D. Luss, Chem. Engrg. Sci. 37 (1982) 1611.
[17] V. Balakotaiah and D. Luss, Chem. Engrg. Sci. 38 (1983) 1709.
[18] V. Balakotaiah and D. Luss, Chem. Engrg. Sci. 39 (1984) 865.
[19] W.W. Farr and R. Aris, Chem. Engrg. Sci. 41 (1986) 1385.
[20] J.B. Planeaux and K.F. Jensen, Chem. Engrg. Sci. 41 (1986) 1497.
[21] R. Ball and B.F. Gray, Ind. Engrg. Chem. Res. 34 (1998) 3726.
[22] D. Drysdale, *Limits of Flammability and Premixed Flames* (Wiley, New York, 1999).
[23] D.L. Baulch, J.F. Griffiths, A.J. Pappin and A.F. Sykes, Combust. Flame 73 (1988) 163.
[24] B.R. Johnson, S.K. Scott and A.S. Tomlin, J. Chem. Soc. Faraday Trans. 87 (1991) 2539.
[25] F.A. Williams, *Combustion Theory*, 2nd ed. (Benjamin, New York, 1985).
[26] M.I. Nelson, H.S. Sidhu, R.O. Weber and G.N. Mercer (under preparation).
[27] H.S. Sidhu, M.J. Sexton, M.I. Nelson, G.N. Mercer and R.O. Weber, in: *Proc. Eng. Math. Appl. Conf.* (2000) p. 251.
[28] B.R. Johnson, J.F. Griffiths and S.K. Scott, J. Chem. Soc. Faraday Trans. 87 (1991) 523.
[29] B.F. Gray, Merkin, G.C. Wake, Math. Comput. Modelling 15 (1991) 25.
[30] E. Balakrishan, M.I. Nelson and G.C. Wake, Math. Comput. Modelling 30 (1999) 177.
[31] F.P. Di Maio, G. Barbieri and P.G. Lignola, J. Chem. Soc. Faraday Trans. 92 (1996) 2989.
[32] R. Seydel, *Practical Bifurcation and Stability Analysis: From Equilibrium to Chaos* (Springer-Verlag, New York, 1994).
[33] E.J. Doedel, T.F. Fairgrieve, B. Sandstede, A.R. Champneys, Y.A. Kuznetsov and X. Wang, AUTO97: Continuation and bifurcation software for ordinary differential equations (with HomCont) (1998).
[34] Y.A. Kuznetsov, *Elements of Applied Bifurcation Theory* (Springer-Verlag, New York, 1998).
[35] B.F. Gray and J.C. Jones, Combust. Flame 57 (1984) 3.
[36] B.F. Gray and L.K. Forbes, Proc. Roy. Soc. London Ser. A 443 (1994) 621.
[37] H.S. Sidhu, L.K. Forbes and B.F. Gray, Proc. Roy. Soc. London Ser. A 449 (1995) 493.
[38] J. Tóth, J. Math. Chem. 25 (1999) 393.
[39] D.P. Copperthwaite, J.F. Griffiths and B.F. Gray, J. Phys. Chem. 95 (1991) 6961.
[40] B.F. Gray and M.J. Roberts, Proc. Roy. Soc. London Ser. A 416 (1988) 361.
[41] D.B. Spalding, Proc. Roy. Soc. London Ser. A 240 (1957) 83.